#3

# INVESTIGATION OF ANODE STRUCTURE IN A RISING-SUN MAGNETRON

R. R. MOATS

LOAN COPY only

TECHNICAL REPORT NO. 99

MAY 18, 1949

RESEARCH LABORATORY OF ELECTRONICS
MASSACHUSETTS INSTITUTE OF TECHNOLOGY

The research reported in this document was made possible through support extended the Massachusetts Institute of Technology, Research Laboratory of Electronics, jointly by the Army Signal Corps, the Navy Department (Office of Naval Research) and the Air Force (Air Materiel Command), under Signal Corps Contract No. W36-039-sc-32037, Project No. 102B; Department of the Army Project No. 3-99-10-022.

MASSACHUSETTS INSTITUTE OF TECHNOLOGY

Research Laboratory of Electronics

Technical Report No. 99 May 18, 1949

# INVESTIGATION OF ANODE STRUCTURE IN A RISING-SUN MAGNETRON

R. R. Moats

## Abstract

Frequency separation between the resonant frequencies of the $\pi$-mode and the nearest other mode may be controlled by varying the ratio of the width at the mouth of the shallower cavities to the width at the mouth of the deeper cavities. To study this problem theoretically, the AX9 18-cavity rising-sun magnetron was chosen as a prototype. A set of computations of resonant frequencies for n = 9 ($\pi$-mode) and n = 8 was carried out, with the dimensions of the deeper cavities held constant, and with the shallower set taken as rectangular slots of various widths. For each width of these slots, a depth was chosen to maintain the $\pi$-mode resonant frequency at the same value as in the prototype. Two more sets of computations were carried out in a similar manner, each with a different width of the deeper cavities but with the original depth. The computed results showed less mode separation for greater width of the deeper cavities, and greater mode separation for greater width of the rectangular slots.

A set of model anodes was constructed in order to provide experimental confirmation of the calculations. The model anodes were constructed with the same dimensions of large cavities for each and with various widths of rectangular slots, to correspond with the first set of computations described above. The deviations of the observed resonant frequencies from those calculated were minor, and supported the calculated results in principle throughout.

In order to identify the resonant modes positively, the radial r-f electric field was observed by means of a rotating probe extending a short distance out from the dummy cathode. The n = 9 mode was recognizable by the 18 peaks per revolution in the observed pattern, but the n = 8 mode produced only two major peaks, corresponding to s = 1, where s is the number of cycles of the r-f field variation around the anode. It is shown that the n = 8 mode contains an s = 1 component and that, according to electromagnetic field theory, the s = 1 component will predominate in the neighborhood of the probe.

# INVESTIGATION OF ANODE STRUCTURE IN A RISING-SUN MAGNETRON

## I. INTRODUCTION

The necessity of separating the frequency of the operating mode of a magnetron from that of any other mode has become well established. The $\pi$-mode, in which the oscillations in adjoining cavities differ in phase by $\pi$ radians, is generally accepted as the most desirable, and in an N-cavity magnetron it is characterized by a mode number $n = N/2$ (1)(2). The mode nearest the $\pi$-mode in frequency is usually that for which $n = N/2 - 1$. The rising-sun type of anode structure, in which cavities alternate in depth, is one of the types developed to accomplish separation between modes. Mode separation in such an anode structure has been investigated previously as a function of the ratio of the depth of the larger cavities to the depth of the smaller cavities (3).

The problem dealt with here, on the other hand, is the control of mode separation by holding the larger cavities fixed in size and shape, and varying the width of the smaller cavities, with the depth of the latter adjusted for constant $\pi$-mode frequency. These limitations are experimentally significant, since a series of anodes composed of vanes, in the tips of which the small cavities are milled as rectangular slots, can be prepared with a minimum of machine time.

The prototype for the anode structures studied is the AX9, an 18-cavity high-power X-band rising-sun magnetron (4), the cross section of which is shown in Fig. 1. This magnetron is of particular interest, since the high-power

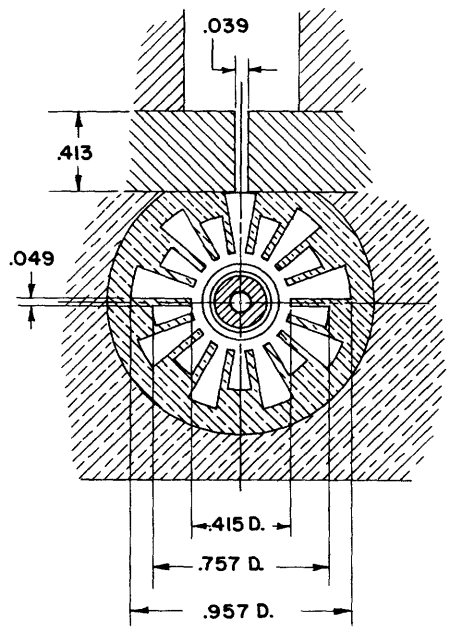


Fig. 1 Cross section of AX9 magnetron (Columbia Radiation Laboratory); dimensions of output slot have been modified for smaller waveguide.

S-band magnetrons which are being constructed and tested in this Laboratory are frequency-scaled copies of the AX9 with only minor changes. The modified anode structure, described above, is shown in Figure 2.

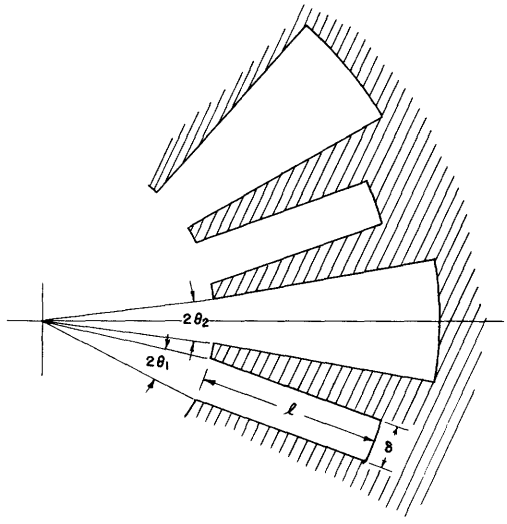


Fig. 2 Cross section of modified rising-sun anode.

## II. THEORETICAL RESULTS

The theoretical portion of this investigation involved the study of mode separation for various combinations of $\theta_1$ and $\theta_2$ (cf. Figure 1). The studies were made by means of computations for various anode configurations, based on numerical solution of the electromagnetic-wave equations. The method of solving these equations for a rising-sun magnetron has been described in detail by Kroll and Lamb (5) for the case where $\theta_1 = \theta_2$, and the results of the solution for $\theta_1 \neq \theta_2$ have also been given in the same report. The derivation of the latter solution is given in Section I of the Appendix of this Report.

A number of independent solutions of the wave equation for a magnetron anode are found. Each of the solutions of interest in magnetron operation is characterized by a mode number n, where n is some integer from one to N/2, inclusive, and N is the number of cavities around the periphery of the anode. The phase of the r-f electric field across the mouth of the $j^{th}$ cavity is given by the expression

$$\exp\left(\frac{2\pi i n}{N} j\right) \quad .$$

In studying the resonances for various values of $\theta_1$ and $\theta_2$, it was desired to hold the $\pi$-mode ($n = N/2 = 9$) resonant wavelength constant at 3.15 cm (which is also the resonant $\pi$-mode wavelength for the AX9) and to study the variation in wavelength of the $n = 8$ mode. The $\pi$-mode wavelength was held constant by adjusting $\ell$. In the first series of computations, the

dimensions of the large cavities were identical throughout with those of the corresponding cavities of the AX9 ($\theta_2 = 0.0715$), and the necessary values of $\ell$ were computed for various values of $\theta_1$. A second and a third series of similar computations were made for $\theta_2 = 0.1227$ and $\theta_2 = 0.1745$, respectively. The required value of $\ell$ as a function of $\theta_1$ for each of the three values of $\theta_2$ is plotted in Figure 3. These results show that as $\theta_1$ approaches zero, the slot depth must approach one-fourth of a free-space wavelength.

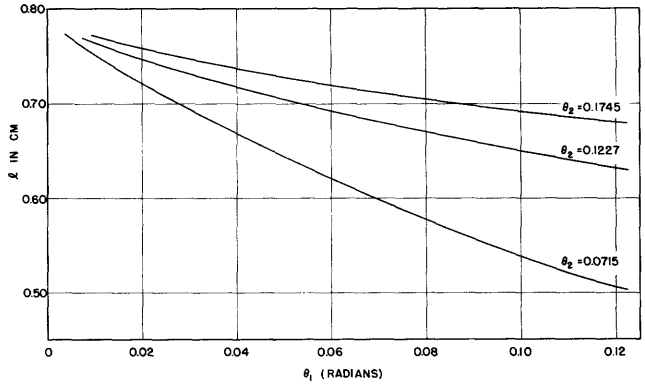


Fig. 3 Slot depth as a function of slot width in modified rising-sun anode.

Using the anode dimensions established by the above calculations, the corresponding values of wavelength for n = 8 were determined, and these are plotted in Figure 4. They indicate that greater mode separation corresponds to wider small slots and to narrower large cavities, and that mode separation tends toward zero as the smaller slots become very narrow. The latter condition approaches a field pattern equivalent to the n = 0 mode in a nine-cavity magnetron, with an open circuit (produced here by the short-circuited quarter-wave slots) between cavities.

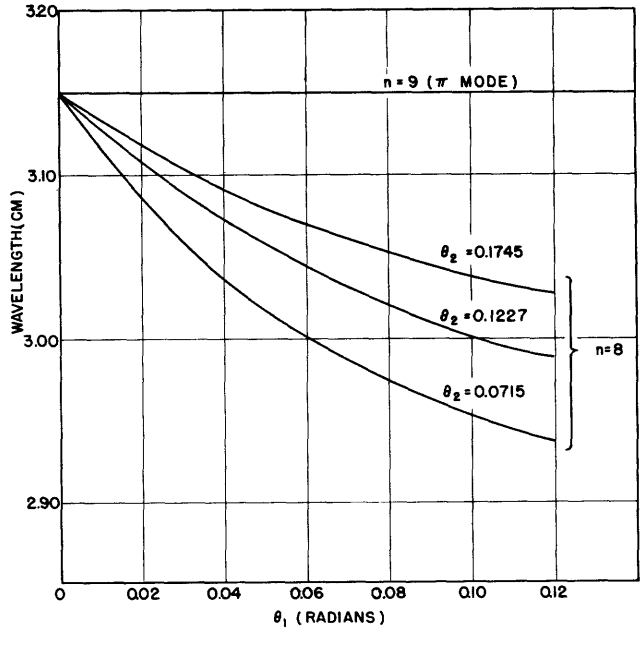


Fig. 4 Calculated resonances in modified rising-sun anode.

## III. MODEL-ANODE TESTS

### A. Equipment

In order to check the above results experimentally, a series of brass model anodes was constructed. The first was a replica of the AX9 anode, and five more were constructed with cross sections of the form shown in Figure 2. Each of the latter five was constructed with a different slot width, with slot depth designed to correspond with the slot width according to Figure 3, and with $\theta_2 = 0.0715$, as in the AX9. Below is a table of slot widths and the corresponding slot depths as measured on the completed anodes.

Table I

| Slot Width $\delta$ (inches) | $\theta_1$ (radians) | Slot Depth $\ell$ (inches) |
|---|---|---|
| 0.0161 | 0.039 | 0.267 |
| 0.0246 | 0.059 | 0.246 |
| 0.0307 | 0.074 | 0.233 |
| 0.0406 | 0.098 | 0.217 |
| 0.0470 | 0.113 | 0.206 |

Figure 5(a) is a photograph of the model anode built as a replica of the AX9, and 5(b) is a photograph of one of the series of five which were built with rectangular slots. In each case, the end caps were omitted in order to show the interior.

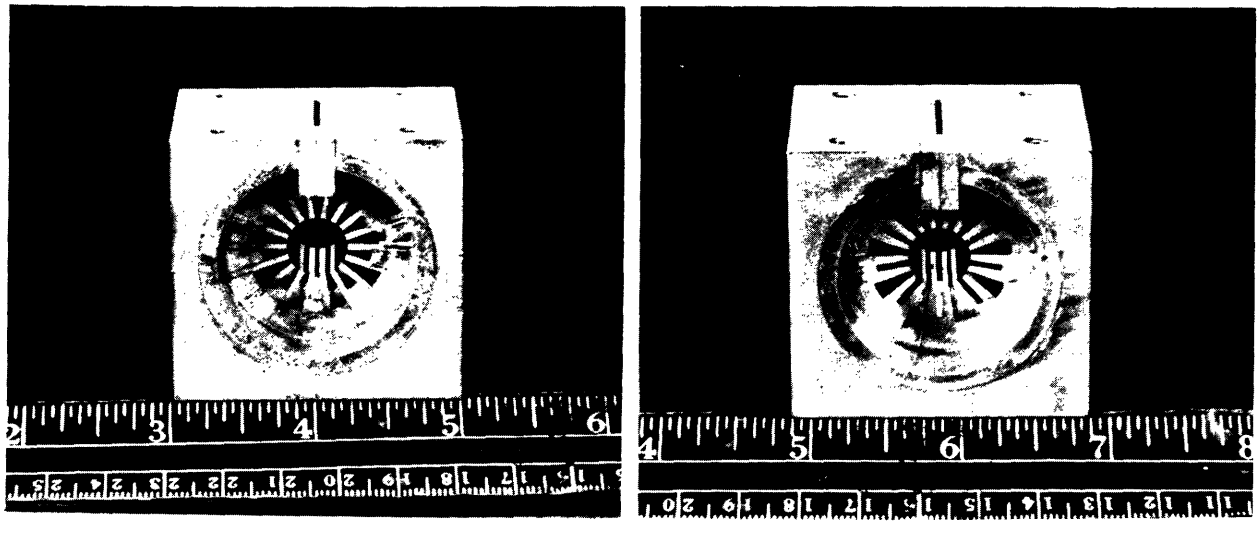

Fig. 5 Model anodes.

(a) Replica of AX9 (cf. Figure 1). (b) Modified rising-sun (cf. Figure 2).

The test equipment, shown in Figure 6, was arranged to supply an X-band signal to the cavity to be tested through a waveguide equipped with attenuator, wavemeter, and slotted section, in order to measure the resonance characteristics of the cavity and to measure the r-f field pattern within the cavity. The r-f signal picked up by the probe was detected,

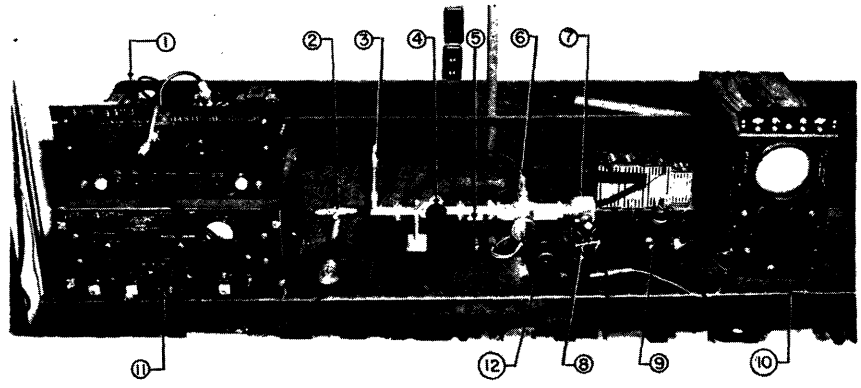


Fig. 6 Equipment for model-anode tests: (1) oscillator and power supply; (2) coaxial wavemeter; (3) line stretcher; (4) variable attenuator; (5) cavity wavemeter; (6) slotted line with traveling probe and detector; (7) model anode; (8) crystal holder and slip-ring assembly; (9) pre-amplifier; (10) cathode-ray oscilloscope; (11) amplifier and standing-wave meter; (12) motor.

the detected signal was led out through slip rings and, after amplification, displayed on the screen of the cathode-ray oscilloscope. The coaxial wavemeter shown in Figure 6 was necessary because the required range of wavelengths extended beyond the range of the cavity wavemeter. However, the latter was preferable in the wavelength range in which it could be used, since the coaxial wavemeter was designed primarily for S-band measurements.

In order to assure correct identification of modes, a rotating probe was constructed to investigate the nature of the r-f field as a function of azimuth.

Figure 7 is a photograph of the components of the rotating-probe assembly and end caps. The probe extends into the cavity from a brass tube which serves as the outer conductor of a coaxial line, and from which it is

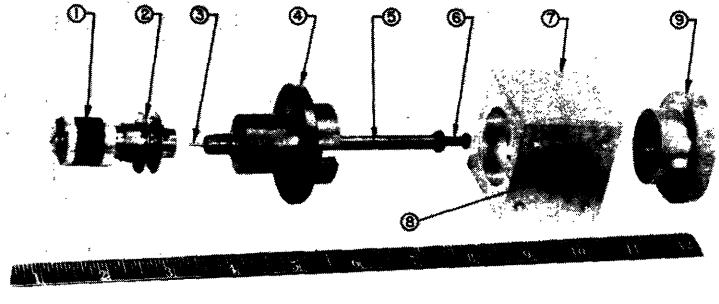


Fig. 7 Components of rotating probe assembly: (1) crystal holder and slip-ring assembly; (2) pulley; (3) center conductor of coaxial line; (4) end cap; (5) probe; (6) tuning screw; (7) model anode; (8) end cap.

insulated. It is attached to a brass rod forming the inner conductor, which leads to the crystal detector on one end and to a tuning screw which short-circuits the line at the other end. The outside diameter of the tube is approximately the same as that of the AX9 cathode, and so should replace it electrically for all of the normal magnetron modes. However, the brass tube makes electrical contact with both end caps, while the magnetron cathode is insulated from the end cap through which it passes and is separated from the other end cap. Therefore, any resonances involving the end spaces may be expected to be altered.

It was found that the voltage output of the detector was so small that the amplification provided by the oscilloscope was insufficient. The necessary additional amplification was accomplished by using a triode (6SQ7) in a circuit designed with special attention to low frequencies. Since the motor was rated 1200 rpm, and the pulley on the probe assembly was the same size as that on the motor, the fundamental frequency was about 20 cps. Battery power was required for both filament and plate in order to eliminate 60-cycle ripple.

The output signal of the preamplifier was connected to the input of the vertical-deflection amplifier of the oscilloscope. The horizontal sweep was synchronized with the rotation of the probe by means of a permanent magnet on the tuning-screw end of the rotating-probe assembly, with the rotation of the magnet generating the synchronizing voltage in a stationary pickup coil. Therefore the vertical deflection on the screen was proportional to the detected signal and the horizontal deflection proportional to the azimuth of the probe.

B. Procedure and Results

In most cases, resonances were located by tuning the oscillator for minimum standing-wave ratio, although a very few were located by observation of the nature of the pattern on the screen. When a resonance was found, the pattern on the screen generated by the rotating probe was observed and photographed, and it was possible to identify the mode corresponding to the resonance by the nature of the pattern.

Results of the tests locating the resonant wavelengths of the $n = 9$ and $n = 8$ modes in each model anode are plotted in Figure 8, along with the theoretical results for $\theta_2 = 0.0715$ (cf. Figure 4). The data in Figure 8(b) are more readily evaluated than those in 8(a) because of small but appreciable variations in the wavelengths at $\pi$-mode resonance; it is the separation in frequency which is significant in this investigation. Agreement with the theoretical values is quite reasonable, considering the unavoidable inaccuracies in the construction of the model anodes and the assumptions made in the calculations.

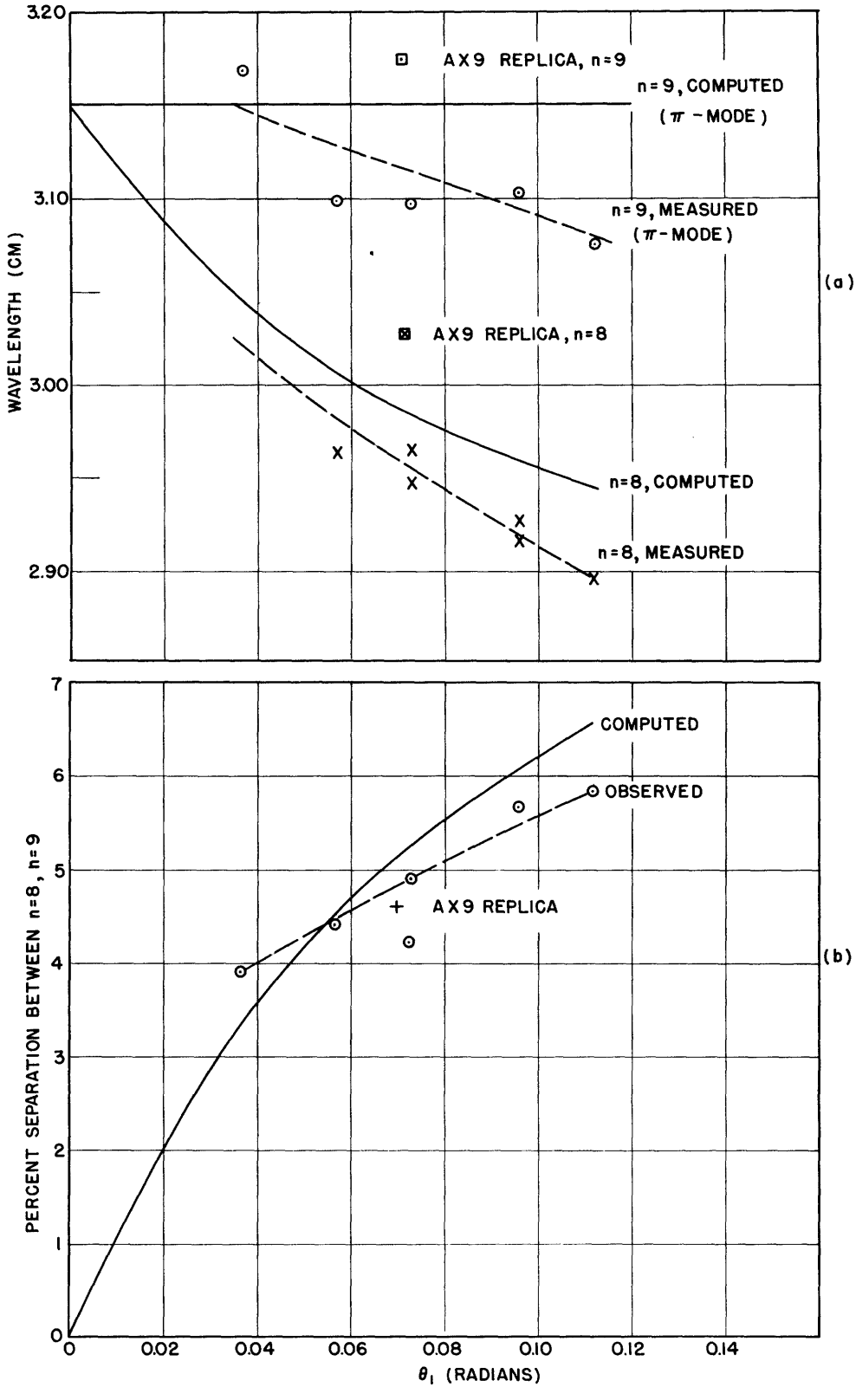


Fig. 8 Resonances in model anodes.
(a) Wavelengths. (b) Mode separation (per cent).

In each of two model anodes, two different resonant wavelengths were identified as corresponding to n = 8. It has been shown that the solution of the wave equations in a multi-cavity anode block is degenerate for all modes except those corresponding to n = 0 and n = N/2, if there is no coupling to the external circuit. When one of the cavities is coupled to a load, the degeneracy is removed, but there are now two distinct and independent solutions possible for each mode number n (except zero or N/2), giving rise to the so-called doublet modes. Any asymmetry, including that produced by the coupling to the load, may be sufficient to separate these two resonances in wavelength enough so that each may be identified.

So far it has merely been assumed that there were no other modes closer in frequency to the $\pi$-mode than n = 8. This assumption was found to be correct experimentally, since there were no other resonances found in any of the model anodes in the range tested, from 2.90 (or less) to 3.40 cm.

## C. Interpretation of Observed Patterns

Photographs of the patterns observed on the screen are shown in Figure 9. All of the photographs of patterns resulting from the n = 9 mode were made without square-wave modulation, while most of the photographs of the n = 8 patterns were made with square-wave modulation.

In all cases except one, the n = 9 mode of each anode block is clearly identifiable because of the 18 peaks in the detected pattern. (A field with a periodicity of 9 must produce 18 peaks in the rectified pattern.) The one exception is associated with a model anode which was found to have one badly deformed cavity.

The identification of patterns corresponding to n = 8 is much less obvious. It is apparent here that the predominating component in the pattern corresponds to a periodicity of one instead of eight. This result may be explained by examining the expression for the radial r-f electric field in the space between cathode and anode:

$$E_r = -\frac{\mu\omega}{k^2 r} \sum_s sC_s Z_s(kr) e^{is\varphi} \quad , \tag{1}$$

where

$$Z_s(kr) = J_s(kr) - \frac{J_s'(kc)}{N_s'(kc)} N_s(kr) \quad , \tag{2}$$

and $\mu$ = permeability of space; $\omega$ = angular frequency; $k_2 = \omega/v$, where v is the velocity of light in space; $i = -1$; r, $\varphi$ and Z are variables in cylindrical polar coordinates, and $C_s$ is a constant for each value of s.

By using only the first term of each power-series expansion of the Bessel functions of the first and second kind, which make up $Z_s(kr)$, the

Fig. 9 Oscilloscope patterns: detected rotating-probe pattern. All except (a) and (b) are made using model anodes whose structure is of the modified type shown in Figures 2 and 5(b).

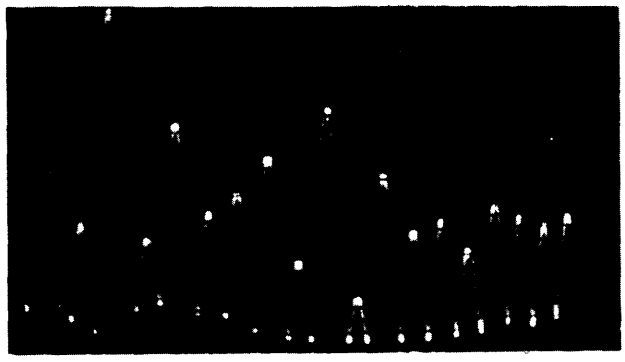

(a) AX9 replica, n = 9.

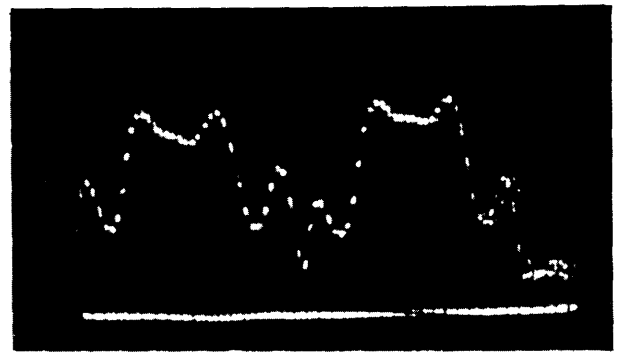

(b) AX9 replica, n = 8.

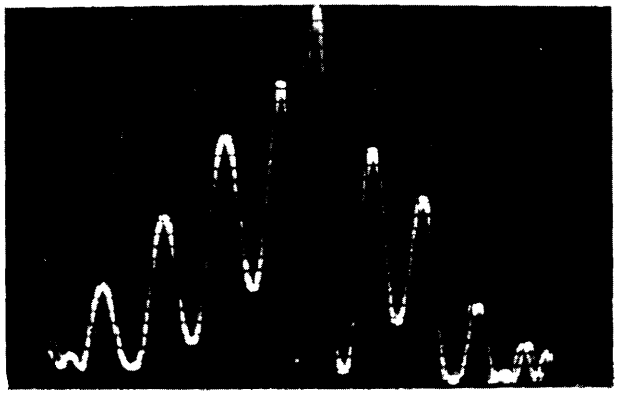

(c) $\theta_1 = 0.039$, n = 9.

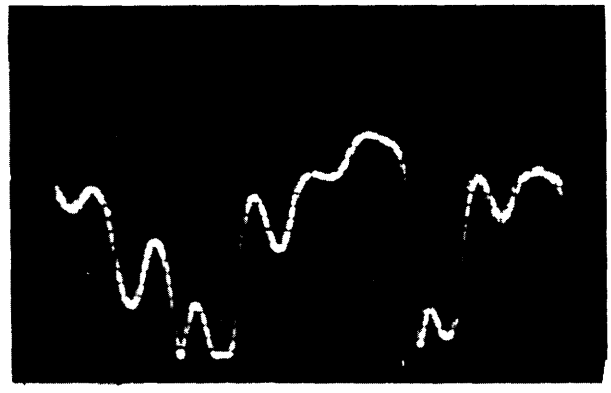

(d) $\theta_1 = 0.039$, n = 8.

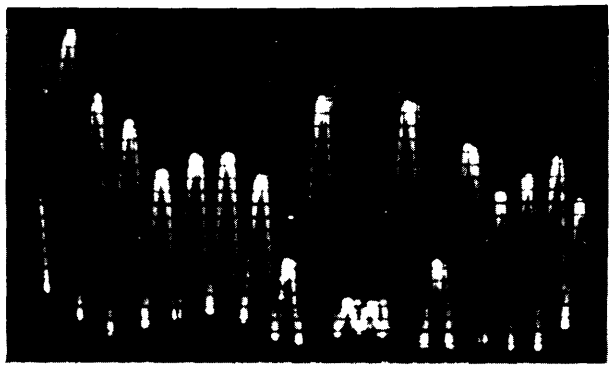

(e) $\theta_1 = 0.057$, n = 9.

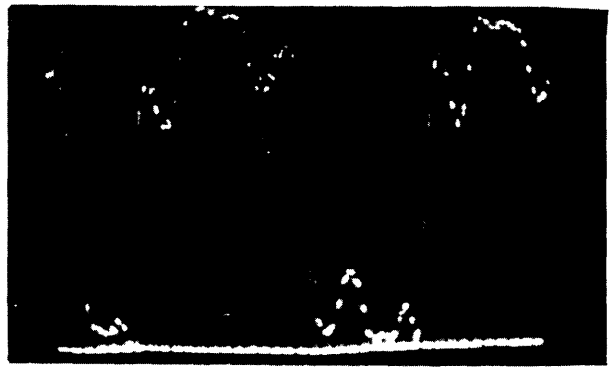

(f) $\theta_1 = 0.057$, n = 8.

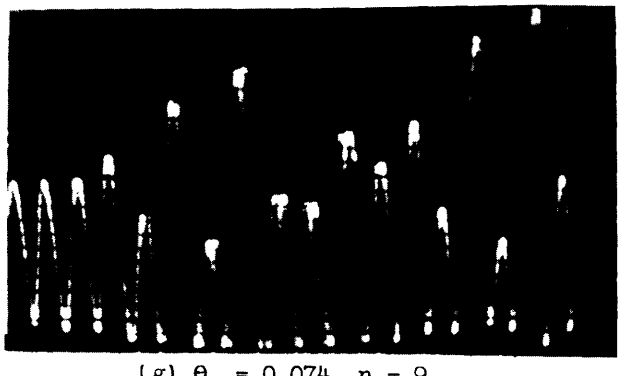

(g) $\theta_1 = 0.074$, n = 9.

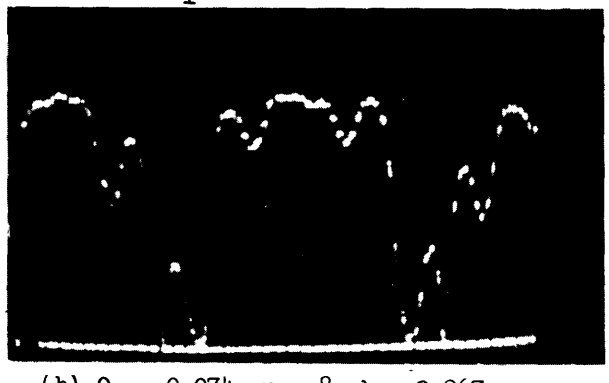

(h) $\theta_1 = 0.074$, n = 8, $\lambda = 2.967$ cm.

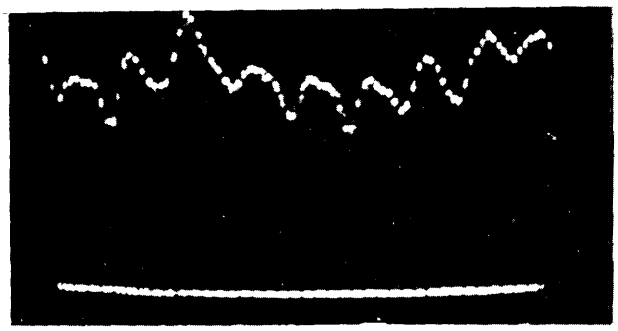

(i) $\theta_1 = 0.074$, n = 8, $\lambda = 2.950$ cm.

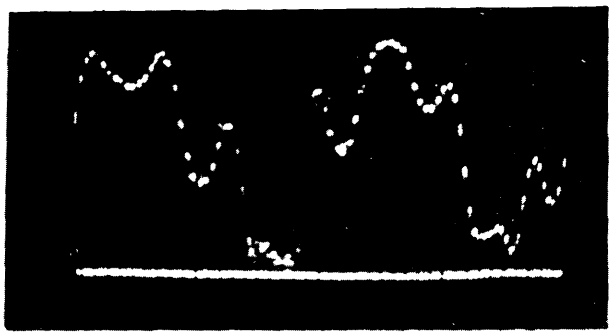

(j) $\theta_1 = 0.074$, n = 8, $\lambda = 2.946$ cm.

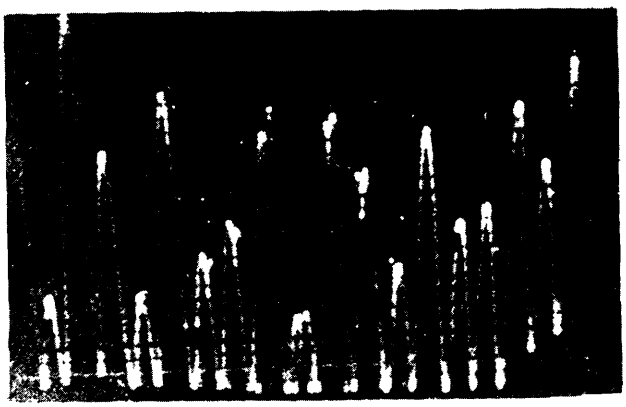

(k) $\theta_1 = 0.096$, n = 9.

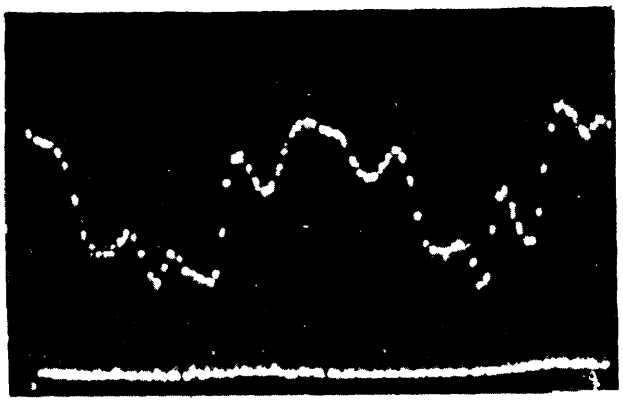

(l) $\theta_1 = 0.096$, n = 8, $\lambda = 2.916$ cm.

(m) $\theta_1 = 0.096$, n = 8, $\lambda = 2.926$ cm.

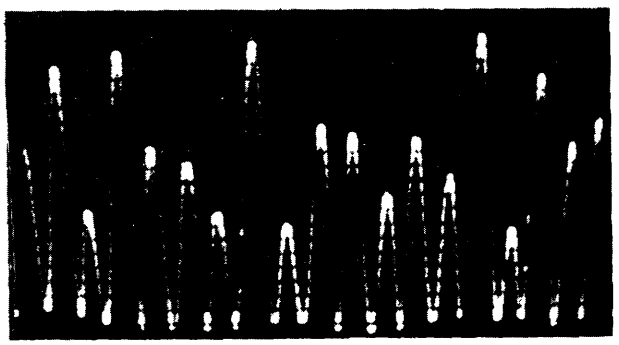

(n) $\theta_1 = 0.112$, n = 9.

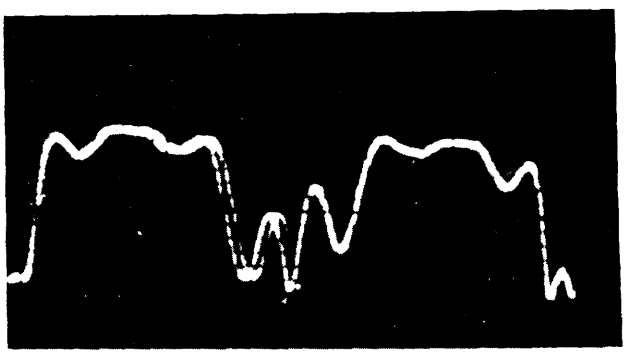

(o) $\theta_1 = 0.112$, n = 8.

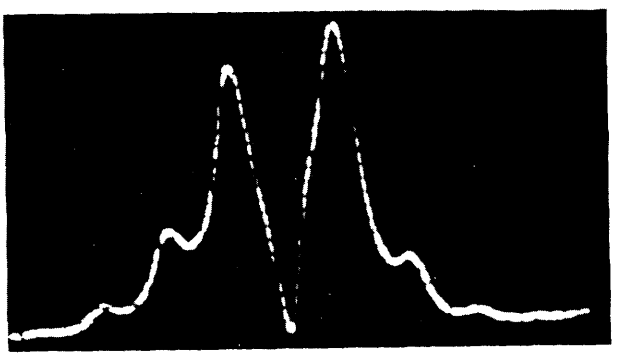

(p) $\theta_1 = 0.096$, no mode, $\lambda = 3.42$ cm.

following approximation is found for the ratio of radial electric field at the anode (r = a) to that at any radius r for a given s:

$$\left.\frac{E_r(r,\varphi)}{E_r(a,\varphi)}\right|_s = \frac{aZ_s(kr)}{rZ_s(ka)} \approx \left(\frac{r}{a}\right)^{s-1}\left[1 + \left(\frac{c}{r}\right)^{2s}\right] \quad . \qquad (3)$$

For n = 8, the values of s which are significant are those corresponding to s = n + m(N/2), where m is a positive or negative integer or zero; therefore, s = 8, 17, 26, etc., and s = 1, 10, 19, 28, etc., omitting the minus sign. (Cf. Eq. (12) Section II, Appendix.) For s = 1, the approximation in Eq. (2) is useful only qualitatively. For s = 8, the values given by (2) are accurate to about 1 per cent.

Equation (2) indicates that the s = 8 component of the electric field is essentially proportional to $(r/a)^7$. On the other hand, $Z_1(kr)/Z_1(ka)$ changes very slowly with r. The probe extends from r = c = 0.6a to approximately r = 0.8a. At the mid-point of the probe (r = 0.7a) the intensity of the s = 8 component of the field is about 0.08 of its intensity at the anode, according to Eq. (2). Using the appropriate Bessel functions according to Eq. (1), the s = 1 component of the field at r = 0.7a is 1.36 of its intensity at the anode. Thus, although the s = 8 component is greater at the anode, it is the s = 1 component which predominates at the probe.

Numerical computations of the radial-field intensity as a function of azimuth have been made as described in Section III of the Appendix, and compared with the results observed experimentally. The expression for $E_r$ in Eq. (1), which includes the factor $e^{is\varphi}$, represents a wave traveling in the positive-$\varphi$ direction (a factor $e^{-i\omega t}$ is therefore implied). A wave traveling in the negative-$\varphi$ direction is equally possible. The method of feeding the signal into the anode system through one cavity leads to two possible combinations of traveling waves to produce a standing wave. In one case, cos s$\varphi$ is substituted for $e^{is\varphi}$ and, in the other, sin s$\varphi$ is substituted.

The best agreement between experimental and computed patterns occurs approximately at r = 0.7a. Plots of these results are shown in Figure 10, where the computed curve of 10(a) is plotted as the sum of a series of terms of the form E sin s$\varphi$, and the computed curve of Figure 10(b) as the sum of a series of terms of the form E cos s$\varphi$, with r = 0.7a and $\theta_1$ = 0.0715 (as in the AX9) in each case. Also included in each of these figures is the observed pattern which most nearly fits the computed pattern, taking the observed patterns from the model anode for which $\theta_1$ = 0.074. The "observed" curves for Figures 10(a) and 10(b) come from Figures 9(h) and 9(j), respectively. On the assumption that the crystal was a square-law detector, the square root of the observed vertical deflection was taken point by point, and the sign reversed where it appeared necessary, thus producing the

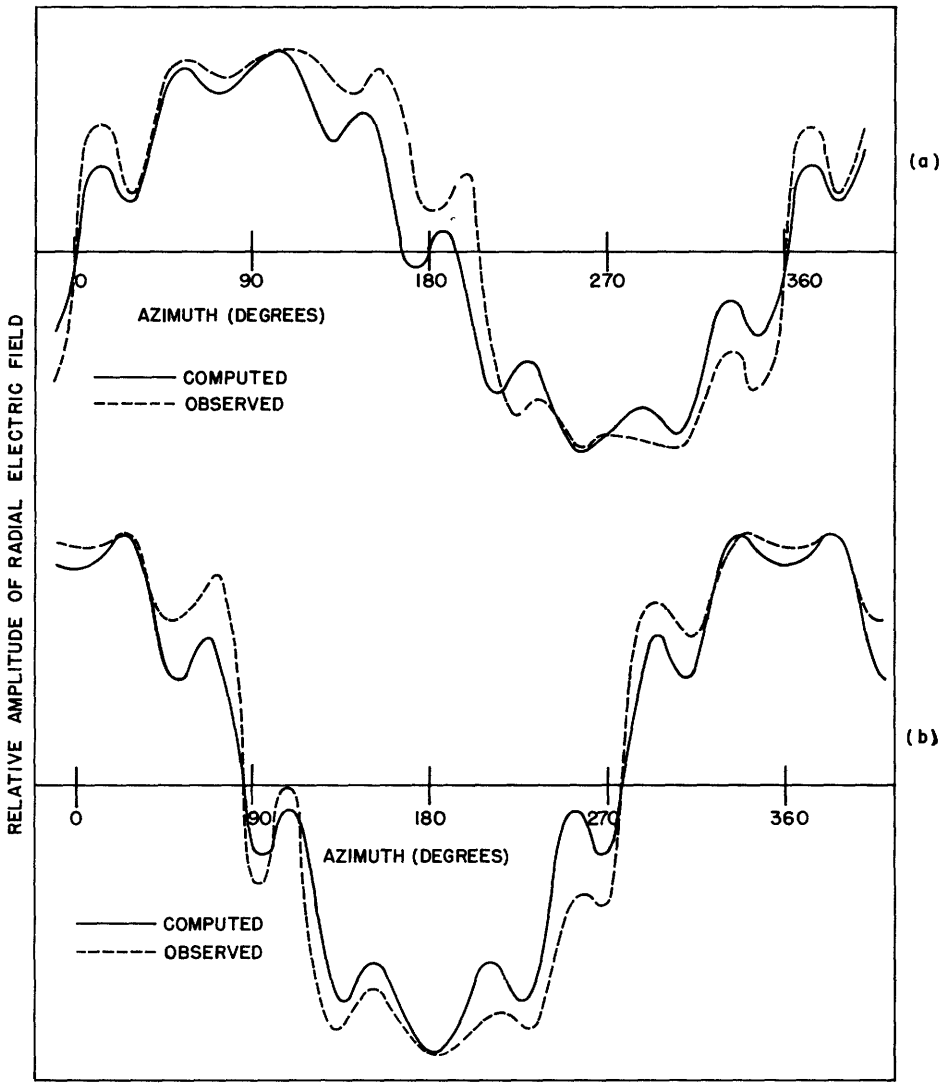


Fig. 10 Comparison of theoretical and observed values of $E_r$ as functions of $\varphi$ at $r = 0.7a$.

(a) $E_r$ represented by summation of terms of the form ($E_s \cos s\varphi$).

(b) $E_r$ represented by summation of terms of the form ($E_s \sin s\varphi$).

"observed" patterns as plotted in Figure 10. Although the quantitative agreement between the experimental and calculated patterns is only fair, it is good enough to furnish satisfactory confirmation of the identification of these two resonances.

The above discussion of the decrease of the intensity of the $s^{th}$ component of a given mode proportionally to $(r/a)^{s-1}$, where s is large, applies equally well to the $n = 9$, or $\pi$-mode. The values of s which are associated with the $n = 9$ mode are $s = 0, 9, 18, 27$, etc. Of these, only the $s = 9$ component is observed, because there is no radial component corresponding to $s = 0$, and the other components are much too small to be observed in the

neighborhood of the probe. However, as a consequence of the fact that the intensity of the s = 9 component is proportional to $(r/a)^8$, the amplitude of the observed signal on the screen was much less than that for n = 8 (dominated by s = 1) for a given power input and gain-amplifier setting. The photographs of Figure 9 which represent the $\pi$-mode were taken with a much higher gain than for the s = 8 mode.

Another effect of the decrease in intensity of higher-order components (i.e., higher values of s) is to amplify the apparent effect of small irregularities in the pattern. A single irregularity in the anode structure, for example, may be expected to manifest itself in the observed $\pi$-mode pattern as a superimposed s = 1 component, with other higher-order components which are less noticeable. As a result of the drastic decrease of the amplitude of the s = 9 component at the probe, the effect of the irregularity appears very large. An extreme case is that shown in Figure 9(c). Examination of the corresponding anode block ($\theta_1 = 0.039$) showed that the mouth of one of the rectangular cavities had been pinched together, making it somewhat narrower than the mouths of the other rectangular cavities in the same anode block. A less drastic example of the same phenomenon is shown in Figure 9(e). Here the contamination is much less severe, and there were no obvious defects of the cavity structure.

It must be taken into account that the output slot, which couples the magnetron anode to the load, constitutes an irregularity. If the load is properly matched, there will be a purely "resistive" irregularity; a mismatch in either the load or the coupling circuit may also introduce a "reactive" disturbance in the field pattern, thus distorting the field pattern by a still greater amount.

There appears to be some tendency for the s = 1 contamination of the $\pi$-mode to be less in anode structures in which $\theta_1$ is greater. Such an observation can be accounted for by the fact that the relative energy storage of the system is greater for larger $\theta_1$, a condition which would tend to reduce the distorting effect of the output slot by increasing the loaded Q or, in other words, by decreasing the proportion of stored energy dissipated in the load per cycle. On the other hand, this observation may be a result of the fact that the relative irregularity of $\theta_1$ from one cavity to the next may be expected to be less when $\theta_1$ is greater.

It is significant that while the values of s associated with the $n^{th}$ mode in a rising-sun anode are given by $s = n + m(N/2)$, the values of s in an anode with all cavities alike (such as a strapped anode) include only those given by $s = n + mN$. (In each case, m includes all positive and negative integers and zero.) Thus, an uncontaminated n = 8 mode in an 18-cavity strapped magnetron, and an $n = N/2 - 1$ mode in an N-cavity strapped magnetron,

would not include an s = 1 component. However, the above discussion of the effect of irregularities, including the coupling to the external circuit, applies equally well to any cylindrical anode structure.

The pattern shown by Figure 9(p), corresponding to the model anode for which $\theta_1 = 0.098$, is typical of the off-resonance patterns. The sharp dip between the two largest peaks was found to correspond with the cavity coupled to the line through which the signal is fed into the cavity. This pattern contains components associated with all values of s. As the frequency of the signal generator is moved toward a resonance, the components associated with that particular resonance become large, and eventually the pattern has the appearance of a wave propagated all around the anode, instead of the appearance of a wave attenuated in both directions from the input cavity as in Figure 9(p).

## D. Length of End Spaces

In another series of tests made on the model anodes, the end spaces were made shorter by filling part of the space with pairs of plates of varying thicknesses and, finally, filling all of the end space. The results shown in Figure 11, taken for the replica of the AX9, are representative of the results found in this series of tests. Until the end spaces become very short, there is relatively little effect on either resonance. However, very short end spaces tend to reduce the $\pi$-mode resonant wavelength, while producing little change in the n = 8 resonance. Thus the mode separation is adversely affected in these latter cases.

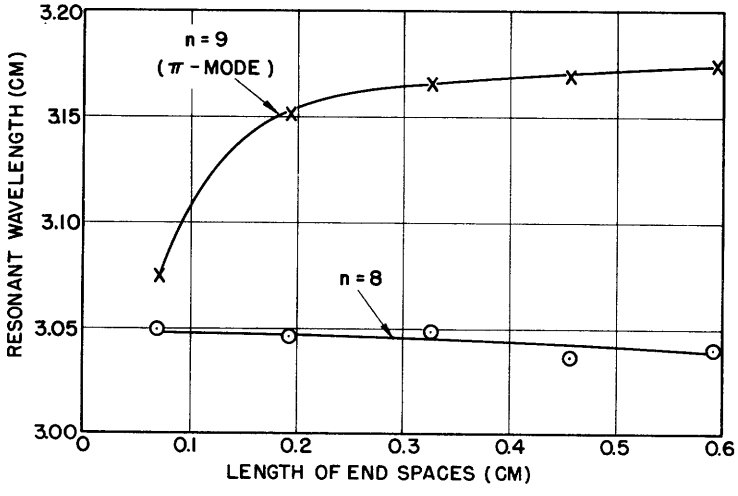


Fig. 11 Effect of length of end spaces upon resonant wavelengths.

When the end spaces were closed up entirely, the $\pi$-mode resonance was shifted so far that it could no longer be reached with available equipment. Under such conditions, the field distribution at the mouth of the cavities can not be uniform, because a finite electric field in the $\varphi$-direction is

not possible at the ends if they are closed by a good conductor. The assumed mode of propagation, the TEM mode, is not possible here and, instead, a waveguide mode is necessary. This should affect quite drastically the $\pi$-mode resonant wavelength, because each cavity must now be excited in a waveguide mode.

## IV. EVALUATION OF RESULTS

The theoretical investigation described in this Report indicates that, in addition to variation of slot depths, the variation of slot widths is also a means of controlling mode separation in a rising-sun magnetron. In general, greater mode separation corresponds to narrower deep slots and to wider shallow slots.

The experimental results obtained in the mode-separation tests provide satisfactory confirmation of the theoretical results. Previous experience in anode design has shown that in order to reach the desired resonant frequency, it is usually necessary first to build either a model for cold-testing or a complete magnetron, and then to make minor changes in order to correct the observed error. On this basis, the agreement between calculated and observed values may be considered reasonably good.

In the case of the mode-separation curves in Figure 8(b), the agreement between computed and observed results is likewise satisfactory. The comparison suggests that the rate of change of mode separation with respect to $\theta_1$ is appreciably less experimentally than theoretically (i.e., the slope of the "observed" curve is less than that of the "computed" curve). However, the number of anodes tested is too small to show conclusive results.

The calculated values of wavelengths may be expected to agree with observed values more closely for relatively long anodes, such as these, than for most anodes. One of the fundamental assumptions made in calculating resonances is that the r-f magnetic field $H_z$ has no variation in the Z-direction ($\partial H_z/\partial z = 0$; see Eq. (3), Appendix, Section I). This assumption implies an infinitely long anode structure. (In the model anodes used in these tests, the anode length is 0.65 of the free-space wavelength for the $\pi$-mode resonance.)

The rotating-probe tests, undertaken for positive identification of modes, confirmed the correctness of the assumed nature of the r-f fields in the space between cathode and anode. They emphasized that the intensity of the $s^{th}$-order component of the radial electric field is approximately proportional to $(r/a)^{s-1}$ for large values of s, and that the s = 8 and s = 9 components, which may be large at r = a, are quite small at r = 0.7a. In the case of the n = 8 mode, the s = 1 component overwhelmed the s = 8 component in the vicinity of the probe; in the case of the n = 9 mode, minor

irregularities, giving rise to lower-order components, affected quite strongly the pattern picked up by the probe.


## ACKNOWLEDGMENTS

The author wishes to acknowledge the contribution of Prof. S. T. Martin, who initiated and supervised the research throughout. He was also responsible for directing the computational work leading to most of the theoretical results.

The author is also grateful for the substantial contributions of Miss Patricia J. Boland, who carried out the extensive computations; of Mr. R. Q. Twiss, who assisted in the theoretical work; of Mr. Walter Rotman, who assisted in the experimental work; and of Dr. D. L. Bendict of Harvard University who made several very valuable suggestions for construction of the rotating-probe system.


## APPENDIX I.

### Calculation of Resonant Wavelengths

In computing the wavelength at which the magnetron resonates in any given mode, all the cavities will be considered as rectangular slots, as shown in Figure 12. The angle subtended by the deeper slots is $2\theta_2$, and the angle subtended by the shallower slots is $2\theta_1$.

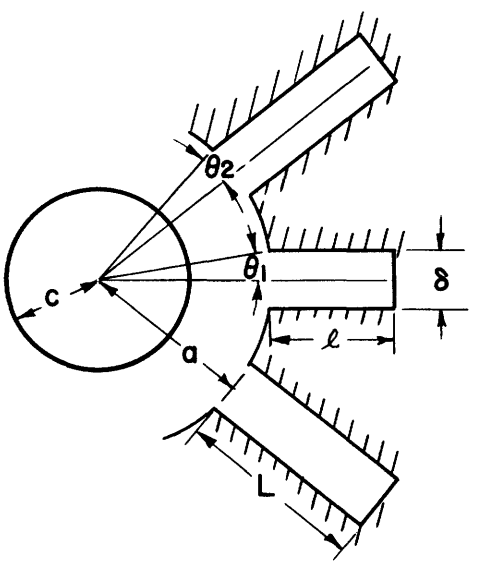


Fig. 12 Cross section of anode–cathode structure used in deriving resonance equations.

In order to determine the electromagnetic field in the cylindrical space between cathode and anode, it is necessary to solve Maxwell's equations in cylindrical coordinates, subject to the boundary conditions imposed by the fields in the 18 rectangular slots and by the cathode. Such a solution

for the rising-sun magnetron has been given by Kroll and Lamb (6) for the case where $\theta_1 = \theta_2$, and the results of the solution for $\theta_1 \neq \theta_2$ are also given. The latter solution is carried out below.

Solution of Maxwell's equations in the cylindrical space between cathode and anode for a resonant mode of the magnetron type, where $H_\varphi = H_r = 0$, and $H_z = H_z(r, \varphi)e^{-i\omega t}$, is of the form

$$H_z = Z_s(kr)e^{is\varphi} \quad , \tag{1a}$$

where $Z_s(kr)$ is a linear combination of Bessel functions of the first and second kinds. The actual complex electric and magnetic fields are then:

$$H_z(r,\varphi) = \sum_s C_s Z_s(kr)e^{is\varphi} \quad , \tag{2a}$$

$$E_\varphi(r,\varphi) = -\frac{i\mu\omega}{k} \sum_s C_s Z_s'(kr)e^{is\varphi} \quad , \tag{3a}$$

$$E_r(r,\varphi) = -\frac{\mu\omega}{rk^2} \sum_s sC_s Z_s(kr)e^{is\varphi} \quad . \tag{4a}$$

At the cathode ($r = c$), the required boundary condition is that $E_\varphi = 0$, and therefore $Z'(kc) = 0$. Therefore

$$Z_s(kr) = J_s(kr) - \frac{J_s'(kc)}{N_s'(kc)} N_s(kr) \quad . \tag{5a}$$

The values of constants $C_s$ in the above expressions are determined by boundary conditions at the inside periphery of the anode ($r = a$). Since the anode in question has cavities with open ends, it is assumed that plane waves propagate in the cavities, that the electric field across the mouth of each slot is uniform and entirely in the $\varphi$-direction, and that the magnetic field is uniform and entirely in the z-direction. On the vane tips between the mouths of the slots, $H_z = E_\varphi = 0$. The magnetic field across the mouth of the $j^{th}$ slot in the $n^{th}$ mode is given by

$$H_z(j) = \alpha \cos k\ell \exp\left(\frac{2\pi i n j}{N}\right) \quad \text{(j even)} \quad , \tag{6a}$$

$$= A \cos kL \exp\left(\frac{2\pi i n j}{N}\right) \quad \text{(j odd)} \quad . \tag{6a'}$$

Here $\ell$ and L are the depths of the shallower and deeper slots, respectively (as shown in Figure 13), and A and $\alpha$ are constants to be determined later. The corresponding values of $E_\varphi$ are:

$$E_\varphi(j) = -\frac{i\mu\omega}{k}\,\alpha\,\sin k\ell\,\exp\left(\frac{2\pi i n j}{N}\right) \qquad (j \text{ even}) \quad , \tag{7a}$$

$$= -\frac{i\mu\omega}{k}\,A\,\sin kL\,\exp\left(\frac{2\pi i n j}{N}\right) \qquad (j \text{ odd}) \quad . \tag{7a'}$$

At the mouths of the slot, the value of $E_\varphi$ determined from the field equations in the cylindrical space between cathode and anode, given by Eq. (2a), must match that determined from the fields in the slots, as given by Eq. (7a) and Eq. (7a'). The fact that $E_\varphi$ as defined from the field in the slot corresponds to a straight line across the mouth of the slot, while $E_\varphi(a,\varphi)$ as defined according to the cylindrical-field solution has a slight curvature, is neglected. The appropriate values of $C_s$ to bring about a match between cylindrical field and slot fields are found as follows:

Let
$$E_\varphi(a,\varphi) = -\frac{i\mu\omega}{k}\,f(\varphi) \quad . \tag{8a}$$

Then $f(\varphi)$ can be represented in a Fourier series (Hartree harmonics (5)) as follows:

$$C_s Z_s'(ka) = \frac{1}{2\pi}\int_0^{2\pi} f(\varphi)e^{-is\varphi}\,d\varphi \quad . \tag{9a}$$

The expression $f(\varphi)$ is determined by matching $E_\varphi$ in Eq. (7a) and Eq. (7a') to $E_\varphi$ in (9). Then

$$f(\varphi) = \alpha\,\sin k\ell\,\exp\left(\frac{2\pi i n j}{N}\right)\,; \quad \frac{2\pi}{N}j-\theta_1 < \varphi < \frac{2\pi}{N}j+\theta_1 \quad (j \text{ even})$$

$$= A\,\sin k\ell\,\exp\left(\frac{2\pi i n j}{N}\right)\,; \quad \frac{2\pi}{N}j-\theta_2 < \varphi < \frac{2\pi}{N}j+\theta_2 \quad (j \text{ odd}) \tag{10a}$$

$$= 0 \qquad \text{elsewhere} \; .$$

Combining Eqs. (9a) and (10a) gives

$$\int_0^{2\pi} f(\varphi)e^{-is\varphi}\,d\varphi = \alpha\,\sin k\ell \sum_{j\ \text{even}} \exp\left(\frac{2\pi i n j}{N}\right) \int_{\frac{2\pi j}{N}-\theta_1}^{\frac{2\pi j}{N}+\theta_1} e^{-is\varphi}\,d\varphi$$

$$+ A\,\sin kL \sum_{j\ \text{odd}} \exp\left(\frac{2\pi i n j}{N}\right) \int_{\frac{2\pi j}{N}-\theta_2}^{\frac{2\pi j}{N}+\theta_2} e^{-is\varphi}\,d\varphi \quad , \tag{11a}$$

or:

$$\int_0^{2\pi} f(\varphi) e^{is\varphi}\, d\varphi = \alpha\, (\sin k\ell)\, 2\theta_1 \frac{\sin s\theta_1}{s\theta_1} \sum_{j\ \text{even}} \exp\left(\frac{2\pi inj}{N}\right) \exp\left(\frac{-2\pi isj}{N}\right)$$

$$+ A\, (\sin kL)\, 2\theta_2 \frac{\sin s\theta_2}{s\theta_2} \sum_{j\ \text{odd}} \exp\left(\frac{2\pi inj}{N}\right) \exp\left(\frac{-2\pi isj}{N}\right) \quad . \tag{12a}$$

The summations of Eq. (12a) may be evaluated as follows:

$$\sum_{j\ \text{even}} \exp\left(\frac{2\pi inj}{N}\right) \exp\left(\frac{-2\pi isj}{N}\right) = \frac{N}{2}\ ,\ s = n + m\frac{N}{2}\ ,$$

$$= 0,\ \text{otherwise}\ ; \tag{13a}$$

$$\sum_{j\ \text{odd}} \exp\left(\frac{2\pi inj}{N}\right) \exp\left(\frac{-2\pi isj}{N}\right) = \frac{N}{2}(-1)^m,\ s = n + m\frac{N}{2}\ ,$$

$$= 0,\ \text{otherwise}\ . \tag{14a}$$

In Eqs. (13a) and (14a), m is a positive or negative integer or zero. If the above results are substituted in (9a),

$$C_s = \frac{N}{2\pi} \frac{1}{Z_s'(ka)} \left[\theta_1 \frac{\sin s\theta_1}{s\theta_1}\, \alpha \sin k\ell + \theta_2 \frac{\sin s\theta_2}{s\theta_2} (-1)^m A \sin k\ell\right] \quad . \tag{15a}$$

The average value of $H_z$ across the slot, where j = 0, is given by

$$\overline{H_z(a,\varphi)}\Big|_{j=0} = \frac{1}{2\theta_1} \int_{-\theta_1}^{\theta_1} H_z(a,\varphi)\, d\varphi = \frac{1}{2\theta_1} \sum_m C_s Z_s(ka) \int_{-\theta_1}^{\theta_1} e^{-is\varphi}\, d\varphi \quad ,$$

or

$$\overline{H_z(a,\varphi)}\Big|_{j=0} = \sum_m C_s Z_s(ka) \frac{\sin s\theta_1}{s\theta_1} \quad . \tag{16a}$$

The average value of $H_z$ above is taken as constant across the slot, as previously discussed. The corresponding value of $H_z$ for j = 1, taking into account that $H_z\Big|_{j=1} = H_z\Big|_{j=0} \exp(2\pi in/N)$, is given by

$$\overline{H_z(a,\varphi)}\Big|_{j=1} = \exp\frac{2\pi in}{N} \sum_m C_s Z_s(ka) \frac{\sin s\theta_2}{s\theta_2} (-1)^m \quad . \tag{17a}$$

In order to solve the two unknown quantities for $A/\alpha$ and for k (and, consequently, for frequency), it is necessary to match the fields only at the slots corresponding to j = 0 and j = 1, since two equations are sufficient

to give a solution for two unknowns. Therefore the values for $H_z$ given by Eqs. (16a) and (17a) match the values given by Eqs. (6a) and (6a'), respectively. If the appropriate value for $C_s$, given by (14), is used, matching Eq. (6a) to (16a) and Eq. (6a') to (17a) gives:

$$\frac{N\theta_1}{2\pi} \sum_m \left(\frac{\sin s\theta_1}{s\theta_1}\right)^2 \frac{Z_s(ka)}{Z_s'(ka)} \alpha \sin k\ell + \frac{N\theta_2}{2\pi} \sum_m \left(\frac{\sin s\theta_1}{s\theta_1}\right)\left(\frac{\sin s\theta_2}{s\theta_2}\right) \frac{Z_s(ka)}{Z_s'(ka)} (-1)^m A \sin kL = \alpha \cos k\ell \quad ; \tag{18a}$$

$$\frac{N\theta_1}{2\pi} \sum_m \left(\frac{\sin s\theta_1}{s\theta_1}\right)\left(\frac{\sin s\theta_2}{s\theta_2}\right) \frac{Z_s(ka)}{Z_s'(ka)} (-1)^m \alpha \sin k\ell + \frac{N\theta_2}{2\pi} \sum_m \left(\frac{\sin s\theta_2}{s\theta_2}\right)^2 \frac{Z_s(ka)}{Z_s'(ka)} A \sin kL = A \cos kL \quad . \tag{19a}$$

Let

$$\sum_1(n) = \sum_{m=-\infty}^{\infty} \frac{Z_s(ka)}{Z_s'(ka)} \left[\frac{\sin s\theta_1}{s\theta_1}\right]^2$$

$$\sum_2(n) = \sum_{m=-\infty}^{\infty} \frac{Z_s(ka)}{Z_s'(ka)} \left[\frac{\sin s\theta_2}{s\theta_2}\right]^2$$

$$\sum_3(n) = \sum_{m=-\infty}^{\infty} \frac{Z_s(ka)}{Z_s'(ka)} \left[\frac{\sin s\theta_1}{s\theta_1}\right]\left[\frac{\sin s\theta_2}{s\theta_2}\right](-1)^m, \quad \text{where } s = n + m\frac{N}{2}$$

Then, from Eqs. (18a) and (19a),

$$\alpha\left[(\sin k\ell)\frac{N\theta_1}{2\pi}\sum_1(n) - \cos k\ell\right] + A \sin kL \frac{N\theta_2}{2\pi}\sum_3(n) = 0 \quad , \tag{20a}$$

$$\alpha \sin k\ell \frac{N\theta_1}{2\pi}\sum_3(n) + A\left[(\sin kL)\frac{N\theta_2}{2\pi}\sum_2(n) - \cos kL\right] = 0 \quad . \tag{21a}$$

When Eqs. (20a) and (21a) are solved simultaneously to eliminate A and $\alpha$ and simplified:

$$\left[\frac{N\sqrt{\theta_1\theta_2}}{2\pi}\sum_3(n)\right]^2 = \left[\cot k\ell - \frac{N\theta_1}{2\pi}\sum_1(n)\right]\left[\cot kL - \frac{N\theta_2}{2\pi}\sum_2(n)\right] . \tag{22a}$$

Solution of (22a) for k will determine the resonant frequency of the

$n^{th}$ mode. The results given in Figures 3 and 4 were obtained by numerical solution of Eq. (22a).

However, in the anode section actually considered, the larger slots are not rectangular but instead are sector-shaped, as shown in Figures 2 and 13. The equivalent length of such a cross section excited in the principal mode has been derived by Kroll and Lamb (7). If the angle subtended by the rectangular slot is equal to that subtended by the sector-shaped cavity, cot kL of Eq.(22) may be replaced by cot $kL_{eq.}$ for any particular value of k, according to the following expression:

$$\cot kL_{eq.} = \frac{J_o(ka')\, N_1(kb') - J_1(kb')\, N_o(ka')}{J_1(ka')\, N_1'(kb') - J_1(kb')\, N_1(ka')} \quad . \tag{23a}$$

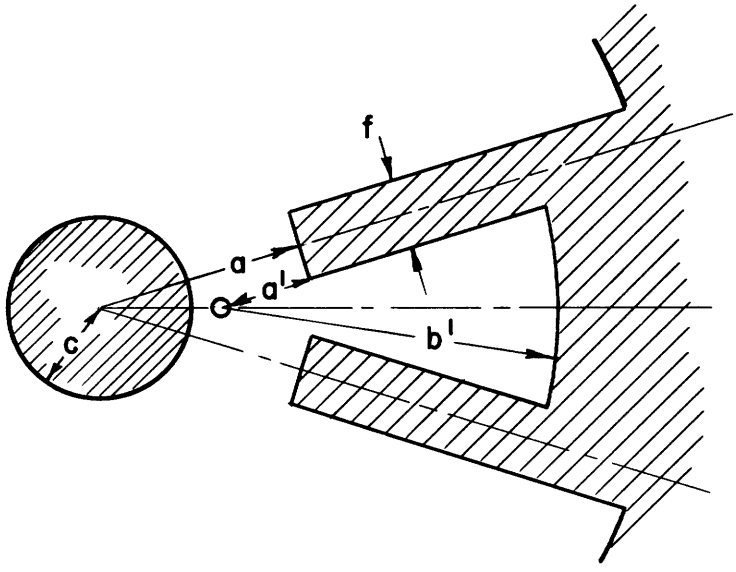


Fig. 13 Cross section of sector-shaped cavities.

## APPENDIX II.

### Radial R-F Electric Field in the Vicinity of the Rotating Probe

The radial electric field is given by:

$$E_r = -\frac{\mu\omega}{rk^2} \sum_s sC_s Z_s(kr)\, e^{is\varphi} \tag{4a}$$

or

$$E_r = -\frac{\mu\omega}{rk^2}\frac{N}{2\pi}\left[\sin k\ell \sum_m \frac{Z_s(kr)}{Z_s'(ka)} \sin s\theta_1\, e^{is\varphi} + \frac{A}{\alpha}\sin kL \sum_m \frac{Z_s(kr)}{Z_s'(ka)} (-1)^m \sin s\theta_2\, e^{is\varphi}\right], \tag{24a}$$

where

$$\frac{A}{\alpha} = \frac{\cos k\ell - (\sin k\ell)\,\frac{N\theta_1}{2\pi}\sum_1(n)}{(\sin kL\,\frac{N\theta_2}{2\pi}\sum_3(n)} \quad \text{(cf. Equation 20).}$$

The expressions $Z_s(kr)$ and $Z_s'(ka)$ are defined as follows:

$$Z_s(kr) = J_s(kr) - \frac{J_s'(kc)}{N_s'(kc)}\,N_s(kr) \quad , \tag{5a}$$

$$Z_s'(ka) = J_s'(ka) - \frac{J_s'(kc)}{N_s'(kc)}\,N_s'(ka) \quad . \tag{25a}$$

If only the first term of the series expansion for each Bessel function of the first or second kind is used:

$$J_s(kr) \approx \left(\frac{kr}{2}\right)^s \left(\frac{1}{s!}\right) \quad ,$$

$$J_s'(kr) \approx \left(\frac{kr}{2}\right)^{s-1}\left[\frac{1}{2(s-1)!}\right] \quad ,$$

$$N_s(kr) \approx -\frac{(s-1)!}{\pi}\left(\frac{2}{kr}\right)^s \quad ,$$

$$N_s'(kr) \approx \left(\frac{s!}{\pi}\right)\left[\frac{2^s}{(kr)^{s+1}}\right] \quad .$$

Therefore

$$Z_s(kr) \approx \left(\frac{1}{s!}\right)\left(\frac{kr}{2}\right)^s + \left(\frac{1}{s!}\right)\left(\frac{2}{kr}\right)^s\left(\frac{kc}{2}\right)^{2s} \approx \left(\frac{kr}{2}\right)^s\left(\frac{1}{s!}\right)\left[1 + \left(\frac{c}{r}\right)^{2s}\right] \quad ,$$

$$Z_s'(ka) \approx \left[\frac{(ka)^{s-1}}{2^s(s-1)!}\right]\left[1 - \left(\frac{c}{a}\right)^s\right] \quad , \tag{26a}$$

or

$$Z_s'(ka) \approx \left[\frac{(ka)^{s-1}}{2^s(s-1)!}\right] \quad , \quad \text{if s is large;}$$

then

$$\left[\frac{Z_s(kr)}{Z_s'(ka)}\right] \approx \left(\frac{ka}{s}\right)\left(\frac{r}{a}\right)^s\left[1 + \left(\frac{c}{r}\right)^{2s}\right] \quad . \tag{27}$$

Therefore, for any particular s,

$$\left.\frac{E_r(r,\varphi)}{E_r(a,\varphi)}\right|_s = \left(\frac{r}{a}\right)^{s-1}\left[1 + \left(\frac{c}{r}\right)^{2s}\right] \quad . \tag{3}$$

The field pattern to be considered is that for n = 8. The values of s which appear in the expression for the n = 8 field pattern are found according to the expression $s = n + m(\frac{N}{2})$ or $s = 8 + 9m$ (cf. Eqs. (13a) and (14a), and therefore include 8, 17, 26, 35, etc., and −1, −10, −19, etc. The values of s in the approximation of (29) must be interpreted as the magnitude of the value of s as given by s = −1, −10, etc. These approximations are correct to within about 1 per cent for s = 8, and for $|s| > 8$ are still more accurate. The numerical computations were based on tabular values for the $|s| = 1$ component, but on Eq. (29) for all other components.

If Laplace's equation is solved for the radial electric field between cathode and anode with the same boundary conditions at the anode and cathode, as described before, the result is identical with the solution of the wave equation if only the first term of the series expansion of each Bessel function of the first or second kind is used.

## REFERENCES


(1) "Microwave Magnetrons", edited by G. B. Collins, (McGraw-Hill Book Co., Inc., New York, 1948), Chapter 4 (L. R. Walker), pp. 118-120.

(2) J. B. Fisk, H. D. Hagstrum, P. L. Hartman, "The Magnetron as a Generator of Centimeter Waves", Bell Sys. Tech. Jour., 25, 221-2, (April 1946).

(3) "Microwave Magnetrons", op. cit., Chapter 3 (N. Kroll) pp. 83-117.

(4) Ibid., Chapter 19 (A. G. Smith) pp. 784-786.

(5) N. Kroll, W. Lamb, "The Resonant Modes of the Rising Sun (A Tube) Anode", National Defense Research Committee, Division H, Report No. 323 (October 25, 1944).

(6) Op. cit.

(7) Op. cit. p. 1.

(8) Op. cit. pp. 34-35.

(9) Op. cit. p. 35.


* * *